Arch Appl Mech (2017) 87:617–631
DOI 10.1007/s00419-016-1212-y

ORIGINAL

Minzu Liang · Xiangyu Li · Fangyun Lu

Modeling the dynamic fracture and fragmentation of explosive-driven metal ring with notches or grooves

Received: 12 September 2015 / Accepted: 22 November 2016 / Published online: 1 December 2016
© Springer-Verlag Berlin Heidelberg 2016

Abstract The dynamic fracture and fragmentation of notched rings under explosive loading were modeled to investigate the fragment characteristics (average fragment size and fragment size distribution) and their effects on fragmentation performance. An analytical model of the average fragment size was proposed for dynamic fracture and fragmentation based on energy criteria related to the material properties, strain rates, and notch effect. The theoretical solutions indicated that the notch effect was dominant with the decreased notch spacing. A law for the fragment size distribution was achieved by combining the binomial distribution. The theoretical distribution depended on the notch spacing, and the distribution was approximated by the natural fragmentation of rings with larger notch spacing. Dynamic fracture and fragmentation experiments were also conducted on cylindrical rings made of AISI 1020 steel. The experimental results were compared with the theoretical models. The average fragment sizes of the theoretical solutions agreed well with the experimental results, and the theoretical distribution provided a good description of the experimental data.

Keywords Notch · Dynamic fracture · Fragmentation · Average fragment size · Fragment size distribution

1 Introduction

The dynamic fracture and fragmentation of rings and cylinders subjected to internal explosive loading continue to be a problem for both armament and civilian applications [1–4]. Modeling the fragmentation process is important for the design, redesign, and efficiency analysis of fragmentation warheads [5–7]. The average fragment size [8,9] and the fragment size distribution [10,11] are two crucial characteristics of the fragmentation phenomenon [12–14].

The seminal modeling of the fragmentation process by Mott is considered a landmark framework for investigating the consequences of the physics of different fractures. Mott attempted to predict the size of the fragments from a cylindrical structure based on the assumptions of a perfect plastic material model and statistical theory. Given the complexity of the underlying physics, the statistical analysis based on experimental results seems to be a promising approach to solve the problem of fragment size distribution [15,16]. Mott [17]

M. Liang · X. Li · F. Lu (✉)
College of Science, National University of Defense Technology, Changsha 410073, People's Republic of China
E-mail: fylu@nudt.edu.cn
Tel: +86073184573267

M. Liang
E-mail: mzliang@nudt.edu.cn

X. Li
E-mail: xiangyulee@nudt.edu.cn

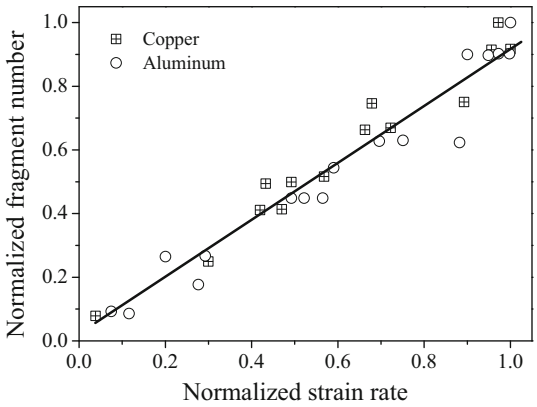

Fig. 1 Representative tests showing normalized fragment number versus normalized strain rate for aluminum and copper ring experiments presented by Grady and Benson

introduced a solution for the propagation of stress release (Mott wave) away from the fracture point, as follows:

$$s = \sqrt{\frac{2Y}{\gamma \rho \dot{\varepsilon}^2}}, \tag{1}$$

where s is the fragment size, $\dot{\varepsilon}$ is the circumferential plastic strain, Y is the yield stress, ρ is the material density, and γ is a parameter that characterizes the microscopic flaws, which caused the variation in strain failure. The Mott model can be usefully abstracted to fragmentation applications, such as a rapidly expanding cylinder or ring [18,19]. The Mott solution was extended by Grady and Kipp [20,21] to consider stress release at the fracture point, wherein the fragment size is twice the distance travelled by the Mott wave:

$$s = \left(\frac{24\Gamma}{\rho \dot{\varepsilon}^2}\right)^{1/3}, \tag{2}$$

where Γ is the energy dissipated in the fracture process. The fundamental difference between the Mott solution and the Grady solution is that Mott was not concerned with the energy dissipated in fracture process [22]. The expanding ring test is always used to validate the energy solution of the Grady's theory [23]. Experiments result in a number of fragments that can be counted. The circumferential length of the ring can divide this number to determine an average fragment length. A one-dimensional ring of material undergoes outward expansion at constant velocity, v. Prior to fracture, the body is uniform with tensile stretching at a strain rate of v/r. This dependence is illustrated in Fig. 1, where the normalized fragment number from similar tests on rapidly expanding aluminum and copper rings is plotted against the radial strain rate imparted to the ring at fracture. Results revealed that the average fragment length is dependent on the mechanical properties of the test material and the dynamic strain rate. Glenn and Chudnovsky [24] modified Grady's theory by introducing a term accounting for the elastic energy before failure, such that the average fragment size becomes

$$s = 4\sqrt{\frac{\alpha}{3}} \sinh\left(\frac{\phi}{3}\right), \tag{3}$$

where

$$\phi = \sinh^{-1}\left[\beta\left(\frac{3}{\alpha}\right)^{3/2}\right], \tag{4}$$

$$\alpha = \frac{3\sigma_c^2}{\rho E \dot{\varepsilon}^2}, \tag{5}$$

$$\beta = \frac{3}{2}\frac{\Gamma}{\rho \dot{\varepsilon}^2}, \tag{6}$$

where E is Young's modulus, and σ_c is the material strength. Glenn and Chudnovsky's theory coincides with Grady's theory at high strain rates [25].

The average fragment size and the fragment size distribution are very important for describing the fragmentation performance. The Mott distribution formula [17], which is the most well known, has been utilized for several decades, wherein the cumulative probability of fragment distribution is given by the following:

$$N(m) = 1 - \exp\left(-m/\mu\right)^{1/2}, \tag{7}$$

where μ is the characteristic fragment mass. This formula has the advantage of its simplicity and faithfully represents majority of the fragment mass distribution in most cases. Several researchers have successfully used this distribution in various forms to organize and compare vast amounts of natural fragmentation data [26–31]. By following Mott's approach based on a Poisson distribution of fracture points, Grady and Kipp [32,33] proposed a simple linear exponential distribution:

$$N(m) = 1 - \exp\left(-m/\mu\right). \tag{8}$$

Moreover, by considering statistically inhomogeneous fragmentation, Grady and Kipp introduced a bilinear expression:

$$N(m) = 1 - \left[f \exp\left(-m/\mu_1\right) + (1 - f) \exp\left(-m/\mu_2\right)\right], \tag{9}$$

where f is the number fraction of the respective homogeneous distributions; μ_1 and μ_2 are the corresponding characteristic fragment masses. Subsequently, Held [34] developed a functional method based on optimization of empirical constants by regression analysis. The relationship between the cumulative mass and fragment number is presented as follows:

$$M(n) = M_0\left(1 - \exp\left(-Bn^{\lambda}\right)\right), \tag{10}$$

where n is the cumulative number of fragments sorted in descending order, and $M(n)$ is the total mass of the fragments. This equation provides a better description of the mass distribution of the projectile. Other excellent fragment mass distribution formulas have also been introduced, such as the lognormal law, Weibull law, and Gilvarry law [35,36].

The models to describe the mass distribution consequences of exploding metal shells were developed by Mott, Grady, and other researchers; these models have been successfully used to describe the fragmentation of cylinders. However, the stress concentration was noticeable at the notch tip when the cylinder was grooved, and the models for cylinders with no obvious defects are not appropriate for the fragmentation of notched cylinders [8,37]. The fragmentation process of notched cylinders is much more complex because of the notch effect [38–40]. In this paper, models are established for the fragmentation of rings with notches. A solution of the average fragment size is proposed based on the energy-based theory of Grady and Kipp; a distribution formula is contributed proposed by combining the binomial distribution. The theoretical models are compared with experimental data, and good correspondences are obtained.

2 Experiment

2.1 Experimental procedures

The developed cylinder experiments were conducted to investigate the notch effect on cylinder fragmentation. The experiment assembly, as illustrated in Fig. 2, is consisted of the plane wave-detonated, explosive-filled, and steel cylindrical rings (specimens). Figure 3 shows a basic test specimen used in the experiments. The cylindrical ring made of AISI 1020 steel has a 110 mm outer diameter, a 5 mm wall thickness, and a height of 5 mm to achieve the approximate plane stress condition [41]. The profile of the notch is U-shaped, with a width of 0.5 mm and a depth of 2.0 mm. Details of the notch pattern for the specimens are given in Table 1. The specimens are filled with explosive TNT.

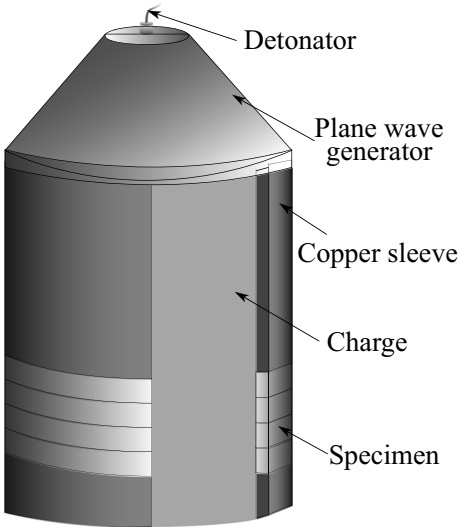

Fig. 2 Schematics of test assembly. The specimens, a stacked set of cylindrical rings made of steel, are filled with main explosive charge, and a copper sleeve is placed before and after the array

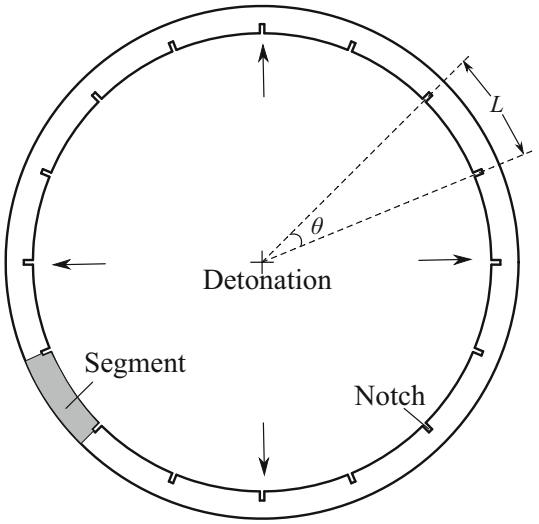

Fig. 3 Geometry of the specimen used in the tests. θ is angle between adjacent notches. L is notch spacing. The part between two adjacent notches is a segment

Table 1 Details of notch pattern for the specimens

Test no	Angle of adjacent notches, θ (○)	Number of segment	Notch spacing, L (mm)
Test 1	11.25	32	10.2
Test 2	30	12	27.2

2.2 Experimental results and analysis

After detonation, the fragments are captured in a large number of sawdust boards. Figure 4 shows the typical recovered fragment photographs of the two tests. Major fragments had in the same size because an attempt was made to control the breakup of cylinders by notching. The fragments in Test 1 are approximately uniform, whereas those in Test 2 dispersed within a certain range. Shear and brittle fractures are the two main types of cracks observed in fragments. The shear fracture face is approximately 45° to the circumference of the wall, whereas the brittle fracture face is along the radial direction of the wall. Moreover, shear failure is a

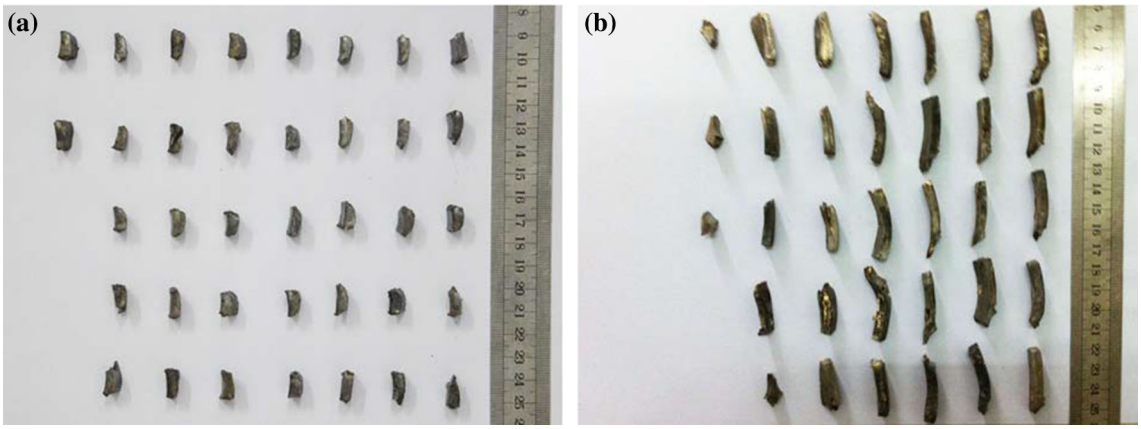

Fig. 4 Photographs of recovered fragments. The notch spacing of specimens in the test 1 and test 2 is 10.2 and 27.2 mm, respectively. **a** Test 1, **b** Test 2

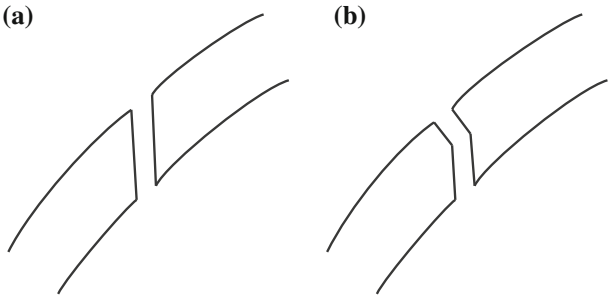

Fig. 5 Brittle and shear fracture of bomb casings. **a** Shear fracture, **b** combined brittle and shear fracture

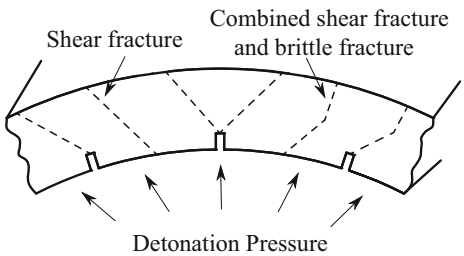

Fig. 6 Schematic of crack types of notched exploded cylinders in the experiments

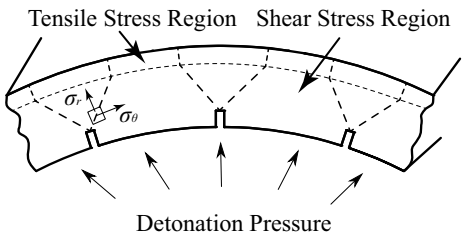

Fig. 7 Crack trajectories in the cylinder. The maximum shear trajectories are approximately at 45° to the circumference of the cylinder wall

localized deformation that can overcome irregularities in the microstructure; brittle failure occurs when too much obstruction for propagation of the shear-banding or on the outer surface of cylinder wall exists because of circumferential tension. A brittle fracture is manifested as a physical cleavage in the material, while adjacent planes in shear-banding remain in contact but flow like fluids over each other. The observation of brittle and

shear fractures in natural fragmentation was reported in the early work of Mott: A shear fracture is shown in Fig. 5a, and a combination of shear and brittle fractures is shown in Fig. 5b. However, both types of cracks were observed in the fragmentation of notched cylinders (Fig. 6). Brittle fracture surfaces usually occur near the outer surface of the case, whereas shear fracture surfaces usually occur near the inner surface.

Shear fracture is empirically the dominant mode in natural fragmentation when the strain rate is high. In this study, shear cracks were more pronounced in fragmentation of those notched cylinders. Hardening initially dominated, but a maximum shear stress was eventually achieved at which the flow changed from stable to unstable at notch roots. The stress near the inner surface appeared to have shear status (Fig. 7). Under the given stress concentration, the maximum shear cracks first emerged at the notch tips. Meanwhile, the response of materials to explosive loading is dependent on the strain rate. The loading strain rate was mainly determined by the detonation pressure, wall thickness, and notch depth. The strain rate increased with increasing detonation pressure, leading to less available time for the diffusion of heat in an area surrounding an irregularity and accelerating shear-banding (especially adiabatic shear-banding) formation. In addition, the shock wave from detonation was a precursory influence. The shock wave, which did not have breaking effects, was reflected from the external surface of the casing as tensile waves. The shock wave loading caused stain hardening because the temporary deformations concentrated the existing crystal structure irregularities and quickly introduced new dislocations in the microstructure. The shock wave disrupted the microstructure, thereby creating a better environment for shear-banding formation [42].

An initial trigger is fixed on the test assembly to record the initial time of dispersion. A series of velocity measurement boards filled with trigger circuits is utilized to record the time the fragments arrive at 3.0 m away from the test assembly. An oscilloscope (OSC) records the electrical signals from the initial trigger and the trigger circuits. The initial velocity of the fragments can be calculated based on the time interval and the distance between the initial trigger and the trigger circuits [43]. Fragments from cylindrical rings decelerate through air according to the well-known law of air resistance. This law can be described by the following exponential equation:

$$v_0 = ve^{\alpha d}, \tag{11}$$

where v_0 is the initial fragment velocity, and v is the fragment velocity at distance d. α is the resistance coefficient, which is calculated as follows:

$$\alpha = \frac{c_f \rho_f s_f}{2M_f}, \tag{12}$$

where ρ_f is the air density; s_f, c_f, and M_f are the cross-sectional area, drag coefficient, and the mass of a fragment, respectively. The drag coefficient can be calculated based on the shape and mass of the recovered fragments.

By integrating Eq. (11) within the fragment dispersion region, the following equation can be obtained:

$$\int_0^t v_0 dt = \int_0^t \left(ve^{\alpha d}\right) dt, \tag{13}$$

which would yield the following:

$$v_0 t = \int_0^t \left(ve^{\alpha d}\right) dt, \tag{14}$$

where $d\,(d) = vdt$.

Thus,

$$v_0 t = \int_0^d e^{\alpha d} d\,(d)\,. \tag{15}$$

Therefore,

$$v_0 = \frac{e^{\alpha d} - 1}{\alpha t}. \tag{16}$$

The value of t is recorded by an OSC, and $d = 3$ m in the tests.

Table 2 Summary of results for the fragments recovered from the cylinder tests

Test no	Initial velocity, v_0 (m/s)	Fracture radius, r_f (m)	Strain rate, $\dot{\varepsilon}$ (s^{-1})
Test 1	1506	0.0663	21732
Test 2	1512	0.0675	21430

The fragments are individually cleaned and measured after retrieval. The logarithmic thickness strain of fragments is calculated by the variety of the thicknesses [44] and could be determined by

$$\varepsilon_{tt} = -\ln(t_f/t_i), \tag{17}$$

where t_i and t_f are the initial and final wall thicknesses of the cylinder, respectively. The failure strain is defined as the effective plastic strain (eps) of the cylinder:

$$\varepsilon_f = \sqrt{\frac{3}{2}\varepsilon_{ij}\varepsilon_{ij}} = \frac{1}{\sqrt{2}}\sqrt{(\varepsilon_t - \varepsilon_h)^2 + (\varepsilon_c - \varepsilon_t)^2 + (\varepsilon_h - \varepsilon_c)^2}, \tag{18}$$

where ε_c and ε_h are the circumference strain and height strain, respectively. By assuming that the strains of circumference and height are not considered, the fracture strain is approximately equal to the logarithmic thickness strain:

$$\varepsilon_f = \varepsilon_t = -\ln(t_f/t_i). \tag{19}$$

Thus, the strain rate $\dot{\varepsilon}$ of a cylindrical ring is as follows:

$$\dot{\varepsilon} = \frac{d\varepsilon}{dt} \cong \frac{v_0}{r_f}, \tag{20}$$

where r_f is the cylinder radius corresponding to fracture completion, which can be calculated as follows:

$$r_f = r_i e^{-\varepsilon_f}, \tag{21}$$

where r_i is the initial cylinder radius.

By substituting Eqs. (16) and (21) into Eq. (20), we obtain the following:

$$\dot{\varepsilon} = \frac{e^{\alpha d_0} - 1}{\alpha t_0 r_i e^{-\varepsilon_f}}. \tag{22}$$

According to Eq. (22), the approximate strain rates can be obtained for fracture processes in the tests. Table 2 summarizes the experimental results of the fragments; the strain rate is approximately $2.0 \times 10^4/s$.

3 Average fragment size

Mott first proposed the famous theory for the natural fragmentation of metal cylinders. This model considers that the body is a perfectly rigid plastic, which is straining in tension under a constant flow stress Y and uniform at a constant stretching rate $\dot{\varepsilon}$. The fractures instantaneously occur at random sites of the Mott cylinder, thereby relieving the tensile stress at the point of fracture to zero. Moreover, the tensile released waves (Mott waves) at the points of fracture, which propagate at finite speeds, relieve the tensile stress in the neighbor region. The theory attempts to capture the characteristic circumferential spacing of fractures. However, the theory does not account for the axial propagation and interaction of cracks within a cylinder of finite length. Subsequently, Grady considered energy dissipated in the fracture process based on Mott's theory and developed an energy-based theory. Both theories focused on the natural fragmentation of exploding cylinders or rings; thus, those theories are unsuitable for solving the fragmentation of a notched cylinder. The present effort is intended to present solutions for the fragmentation of an exploded notched ring based on the theories by Mott and Grady.

As illustrated in Fig. 8, we assumed that prior cracks occur at notches because of the stress concentrations around the notch tips. Fractures are initiated at time $t = 0$ at notch position $h = 0$. The material is uniform at a tensile stress Y in front of the Mott wave, but it is under a constant velocity behind the Mott wave. As soon as the fractures appear at the notches, stress is released in the neighborhood of the said notches. New fractures

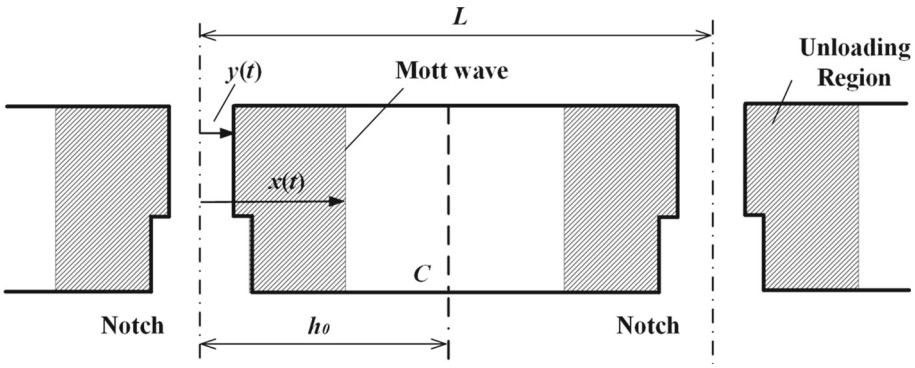

Fig. 8 Mott waves propagate in the controlled fragmentation case wall

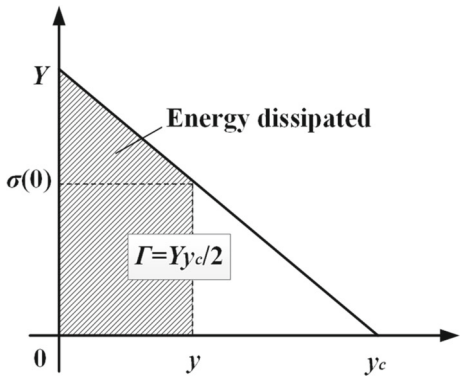

Fig. 9 Dependence of fracture energy on crack-opening displacement

can no longer occur in the released regions. These unstressed waves are called Mott waves. Their traveled distance $x(t)$ depends on the time and physical properties. An arbitrary point C is taken on the circumference of the cylinder at a distance h_0 from the point of fracture (or notch).

The total momentum of the segment within the region $0 \leq h \leq h_o$ is given by

$$I_{0\leq h\leq h_0} = \rho\dot{\varepsilon}x^2 + \int_x^{h_0} \rho\dot{\varepsilon}hdh = \frac{1}{2}\rho\dot{\varepsilon}\left(x^2 + h_0^2\right). \tag{23}$$

According to the theorem of momentum, we obtain the following:

$$\frac{dI_{0\leq h\leq h_0}}{dt} = \sigma\left(h_0\right) - \sigma\left(0\right) = Y - \sigma\left(0\right), \tag{24}$$

where $\sigma(0)$ is the tensile stress of the fracture face, and $\sigma(0)$ is 0 in Mott's theory. Grady considers a model where the tensile stress is gradually reduced over time from $\sigma(0) = Y$ to zero as the crack completely opens. When the crack-open displacement linearly increases from zero to y_c (Fig. 9) [45], $\sigma(0)$ can be expressed as follows:

$$\sigma\left(0\right) = Y\left(1 - \frac{Y}{2\Gamma}y\right). \tag{25}$$

where Γ is the fracture resistance and y is crack-opening displacement. The values of Y and Γ are determined from the static tension tests [18,32].

By substituting Eqs. (23) and (25) into Eq. (24), we obtain

$$\rho\dot{\varepsilon}x\frac{dx}{dt} = \frac{Y^2y}{2\Gamma}, \tag{26}$$

The motion of the crack-opening displacement provides

$$\frac{dy}{dt} = \dot{\varepsilon} x. \tag{27}$$

By combining Eqs. (26) and (27), we can obtain the following:

$$x\,(t) = \frac{Y^2}{12\rho\Gamma} t^2, \tag{28}$$

$$y\,(t) = \frac{\dot{\varepsilon} Y^2}{36\rho\Gamma} t^3. \tag{29}$$

When $y = y_c$, the dissipating energy of the fracture process is given by the following:

$$\Gamma = Y y_c/2. \tag{30}$$

By substituting Eq. (30) into (29), the time at which fracture is complete can be calculated as follows:

$$t_f = \left(\frac{72\rho\Gamma}{\dot{\varepsilon} Y^3}\right)^{1/3}. \tag{31}$$

The coupled Eqs. (28) and (31) give the distances traveled by the Mott wave during the time of fracture, as follows:

$$x_f = \left(\frac{3\Gamma}{\rho\dot{\varepsilon}^2}\right)^{1/3}. \tag{32}$$

The above-mentioned expression indicates that the appearance of natural fragmentation is determined by Γ, ρ, and $\dot{\varepsilon}$. Parameter $\dot{\varepsilon}$ is the loading of the explosive, wherein an increase in loading increases the number of natural fragments. Parameters Γ and ρ belong to the case material properties.

If the notch spacing is $L \leq 2x_f$, the Mott waves release all the materials of the segment between the notches. New fractures can no longer occur in this region during fracture completion. Thus the average fragment size is $x_0 = L$.

If $L > 2x_f$, new fractures may appear. The region without release is as follows:

$$L_{non} = L - 2x_f. \tag{33}$$

Correspondingly, the fragment number of one segment is as follows:

$$n = \frac{L_{non}}{2x_f} + 2 = \frac{L}{2x_f} + 1. \tag{34}$$

Consequently, the average fragment size is as follows:

$$x_0 = L \Big/ \left(\frac{L}{2x_f} + 1\right). \tag{35}$$

In summary, the average fragment size for controlled fragmentation can be obtained as follows:

$$x_0 = \begin{cases} L & (L \leq 2x_f) \\ L \Big/ \left(\frac{L}{2x_f} + 1\right) & (L > 2x_f) \end{cases}. \tag{36}$$

This expression indicates that the solutions are affected by the material properties, loading, and notch effect. If two adjacent notches fracture at time t_f with spacing of less than $2x_f$, these notches will interfere with each other before the fracture growth process is completed. A higher percentage of natural fragments would be achieved by increasing segment size L. When L is much greater than x_f, the average fragment size is as follows:

$$x_0 = L \Big/ \left(\frac{L}{2x_f} + 1\right) \approx L \Big/ \left(\frac{L}{2x_f}\right) = 2x_f, \tag{37}$$

which is approximately equal to the natural fragmentation solution.

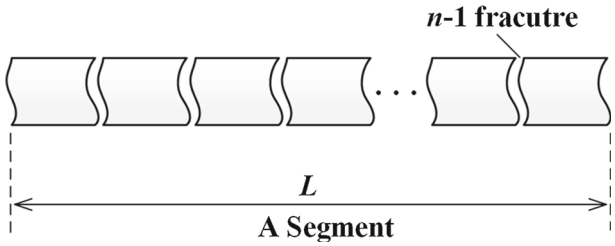

Fig. 10 Cylindrical ring broken at random into fragments of variable length L by $n-1$ fractures

4 Fragment size distribution

The theoretical efforts of Lienau [46] are fundamental to geometric fragmentation. His work considered the elementary problem of an extended body, such as a glass rod or a stretching wire, subjected to forces that cause the multiple fracturing of the said body. If any point on the body has equal likelihood of fracture, the problem is statistically well posed. The problem is modeled as an infinite one-dimensional body or line, wherein breaks are introduced with equal probability at any point. Thus, the random geometric fragmentation of a one-dimensional body appears decidedly unambiguous. The problem of exploded rings could be modeled as an infinite one-dimensional body L, wherein randomly distributed $n-1$ partitions break the body into n fragments. An analytical solution requires only a proper probabilistic description of the random breaks and the lengths of the segments delineated by these breaks.

The binomial distribution is a formula that indicates the probability of achieving a given number of successful outcomes in a predetermined number of statistical trials when the probability of success is the same for each trial. This distribution can be used to describe the probability of getting n - 1 partitions during the breaking of a ring, where each trial has the same probability (Fig. 3). As illustrated in Fig. 10, the problem is modeled as an infinite one-dimensional body L, wherein randomly distributed $n-1$ partitions break the body into n fragments. Given that the distributions of cracks are random events, an analytical solution requires the proper probabilistic description of random fractures. If an arbitrary length l of the body is examined, then the probability of finding $n-1$ fractures within length l can be expressed as the following Poisson distribution:

$$P_{n-1,l}\left(l/\lambda\right) = \frac{\left(l/\lambda\right)^{n-1} e^{-l/\lambda}}{(n-1)!}. \tag{38}$$

where λ is the average spacing between fractures. The Poisson distribution is approximated to the natural fragmentation when n is a large number. However, the n in segment L is generally few. Thus, we proceed with the solution leading to the binomial distribution. The probability of accurately observing j event activations in k trials is

$$P_{j,k}\left(p\right) = \frac{k}{j!\,(k-j)!} p^{j}\left(1-p\right)^{k-j}, \tag{39}$$

where p is the probability of a single activation.

In this study, an arbitrary length l ($l < L$) of the body is examined. According to Eq. (39), the probability not finding fractures within the length l is

$$P_{0,n-1}\left(p_l\right) = \frac{(n-1)!}{0!\,(n-1)!}\left(p_l\right)^{0}\left(1-p_l\right)^{n-1}, \tag{40}$$

where p_l is the probability of a single fracture occurring within the region:

$$p_l = l/L. \tag{41}$$

By substituting Eq. (41) into (40), we obtain the following:

$$P_{0,n-1}\left(p_l\right) = \frac{(n-1)!}{0!\,(n-1)!}\left(\frac{l}{L}\right)^{0}\left(1-\frac{l}{L}\right)^{n-1} = \left(1-l/L\right)^{n-1}. \tag{42}$$

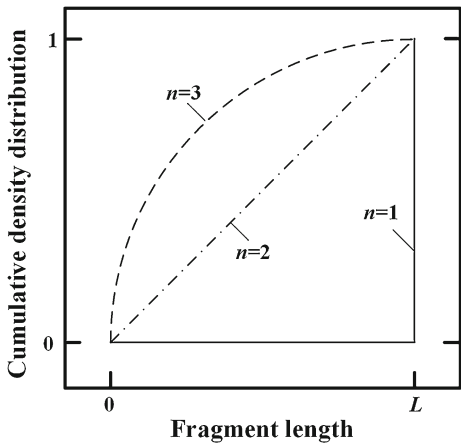

Fig. 11 Fragment size distribution for fragmentation of body. The n is 1, 2, and 3

Table 3 Comparison of the calculated and experimental results

Test no	Distance the Mott wave travels, x_f (m)	Calculated average fragment size (mm)	Experimental average fragment size (mm)	Error (%)
1	10.9	10.2	10.9	6.4
2	11.1	19.8	22.6	12.4

The probability of finding one fracture within the subsequent length increment dl is as follows:

$$P_{1,n-1}\left(p_{dl}\right) = \frac{(n-1)!}{1!\,(n-2)!}\left(\frac{dl}{L-l}\right)^{1}\left(1-\frac{dl}{L-l}\right)^{n-2}. \tag{43}$$

The dl is a relatively small value; thus, Eq. (43) can be simplified to:

$$P_{1,n-1}\left(p_{dl}\right) = \frac{n-1}{L\left(1-l/L\right)}dl. \tag{44}$$

The probability of occurrence of a fragment of length l within an interval dl is as follows:

$$f\left(l\right)dl = P_{0,n-1}\left(p_l\right)\cdot P_{1,n-1}\left(p_{dl}\right), \tag{45}$$

where $f\left(l\right)$ is the fragment size probability density distribution. Equations (42), (44), and (45) can be combined to obtain the following:

$$f\left(l\right) = \frac{n-1}{L}\left(1-l/L\right)^{n-2}. \tag{46}$$

By integrating Eq. (46), the cumulative density distribution can be obtained as follows:

$$F\left(l\right) = \int_0^l f\left(l\right)dl = 1-\left(1-l/L\right)^{n-1}. \tag{47}$$

Figure 11 compares the probability density curves for different numbers of breaks. Therefore, the fragment size probability distribution depends on the body length L according to Eq. (47). Moreover, the probability density curves are approximated by the Poisson distribution when n is a large number.

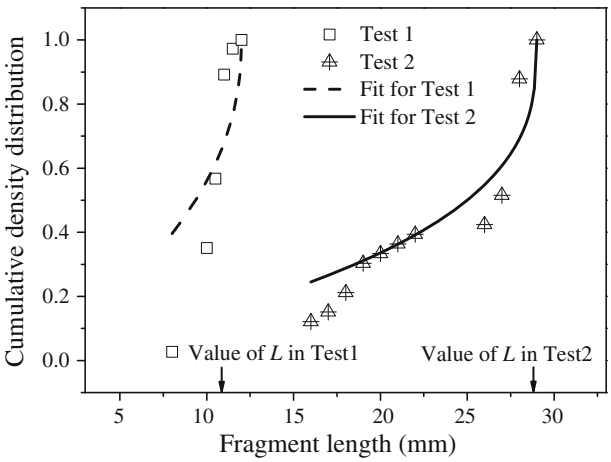

Fig. 12 Fragment size distributions for the pit tests

5 Comparison with experimental data

By combining the material density, fracture energy dissipation, and strain rate, we obtained the distance travelled by the Mott wave in Eq. (32). The calculated and experimental results are compared in Table 3. The experimental results of Test 1 are in good agreement with the theoretical solutions. The error in Test 2 reached 12.4% and can be attributed to the measurement of the velocity and fragment parameters. However, the errors are acceptable in explosive-driven cylinder experiments. Figure 12 shows the experimental results of the fragment size distribution. Given the relative simplicity of the distribution model, the accuracy of the theoretical predictions is in good agreement with the experimental data.

6 Discussion

The fracture process can mainly be broken down into three steps. First, initial stress in cylinders is caused by explosive shock waves when the explosive is detonated, causing rapid outward acceleration. The cylinder is extruded by the magnitude shock wave to make wall thinning. The shock wave from detonation is a precursory influence. The shock wave, which does not have breaking effects, is reflected from the external surface of the casing as tensile waves. The shock wave loading results in stain hardening as temporary deformations concentrating existing crystal structure irregularities and introducing new dislocations in the microstructure quickly. The shock wave disrupts the microstructure, leading a better environment for shear-banding formation. Then the wall is turned into tensile after the detonation pressure pass by the cylinder. The stress near the case inner surface appears shear status. Owing to stress concentration, the cracks firstly emerge at notch tips. The detonation pressure leads to less time available for diffusing of heat in an area surrounding an irregularity, and accelerating shear-banding (especially adiabatic shear-banding) forming. Cracks form and grow from the root of notches, begin to propagate through the wall after a very short time. Finally, gas products begin to vent as cracks propagate completely through the wall.

It is apparent that if two fractures initiate within a time t_f and with spacing between them of $<2x_f$, they will interfere with each other before the fracture growth process is complete. Thus, critical notch spacing for fragment distribution is x_c:

$$x_c = 2x_f = \left(\frac{24\Gamma}{\rho\dot{\varepsilon}^2}\right)^{1/3}. \tag{48}$$

The distance x_f traveled by Mott waves in the fracture process was half of the distance between adjacent notches s. In other words, natural fragmentation did not appear when $s \leq x_c$. It is indicated that appearance of natural fragmentation is determined by Γ, ρ, and $\dot{\varepsilon}$. Parameter $\dot{\varepsilon}$ is referred to the loading of explosive. An increase in the loading evidently resulted in increased number of natural fragments. Parameters Γ and ρ belong to the case material properties. High percentage of controlled fragments was achieved with increasing Γ or decreasing the ρ.

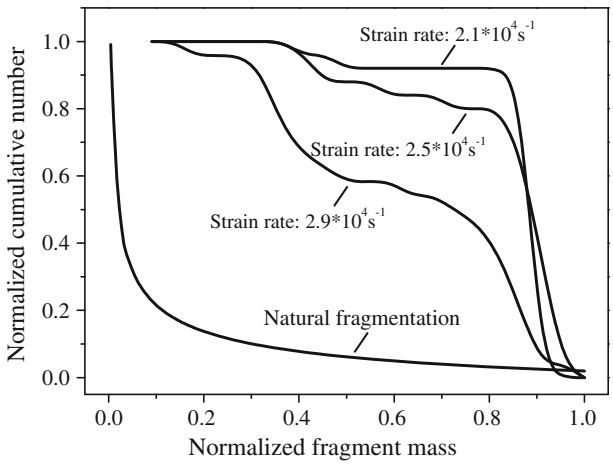

Fig. 13 Cumulative fragment mass distributions for natural and controlled fragmentation

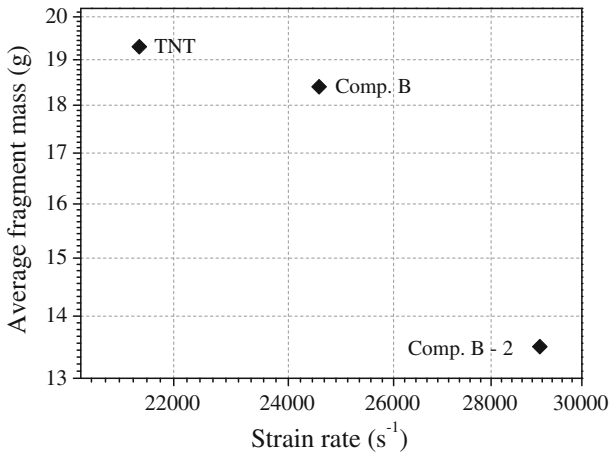

Fig. 14 Effect of strain rate on the average fragment mass

Experimental results indicated that the effects of notches in cylinder walls are sensitive to deformation behavior. The notch effects on fragmentation are small at high strain rates but become noticeable at lower strain rates (Fig. 13). The released regions close to the notches reflect the notch effect of cylinders. The fragmentation of the unreleased region followed the natural fragmentation law. More unreleased areas were achieved by increasing the strain rate loading (Fig. 14). Meanwhile, the fragmentation of unreleased regions obeyed a statistical law. According to analytical models of natural fragmentation, the average fragment size decreases with increasing strain rate. In conclusion, the unreleased region increased and average fragment size decreased with increasing strain rate loading, and a higher percentage of natural fractures appeared between notches. However, the proposed analysis of the circumferential fracture was a one-dimensional model, which was not appropriate for the complex biaxial fragmentation terms. A few axial and corner fractures also appeared in the cylinders. The circumferential strain rates were larger than the axial strain rates in most regions of the cylinders; the axial strain to failure occurred later than in the circumferential direction.

7 Conclusion

We developed models for dynamic fracture and fragmentation of cylindrical rings with notches under explosive charge. The models are based on a reasonable assumption that prior cracks occur at notches because of stress concentrations around the notch tips. The fracture process is modeled by combining Mott's and Grady's fragmentation theories. Fracture solutions, including compete time, Mott wave travels, fragment number and average fragment size, are obtained. The solutions are approximated to results of natural fragmentation when

the L is much greater than x_f. Fractures that are more natural appear with increasing notch spacing. Moreover, the expression of fragment size probability density distribution and cumulative density distribution is acquired using the binomial distribution. The distribution is much more dependent on notch spacing, which is different from the natural fragmentation of ring. The probability density curves are approximated to the Poisson distribution when the notch spacing is long enough.

Dynamic fracture and fragmentation experiments are conducted on cylindrical ring made of AISI 1020 steel. Fragments are recovered, and velocities are measured. The average fragment sizes of the theoretical solutions are acceptable compared with the experimental results. In addition, the theoretical distributions are compared with the experimental data, and good agreements are obtained. However, the models put forward in this study are one-dimensional models, which are not appropriate for the complex biaxial fragmentation terms. Further investigation should focus on modifying presented model to achieve a 2D analysis, which would enable the more realistic prediction of the notched cylinder fragmentation process.

Acknowledgements The authors would like to acknowledge the financial supports by the China National Natural Science Funding (11202237 & 11132012).

References

1. Villano, D., Galliccia, F.: Innovative technologies for controlled fragmentation warheads. J. Appl. Mech. **80**(3), 1–9 (2013)
2. Arnold, W.: Controlled fragmentation. In: Shock Compression of Condensed Matter. AIP Conference Proceedings, pp. 527–530 (2002)
3. Martineau, R.L., Anderson, C., Smith, F.: Expansion of cylindrical shells subjected to internal explosive detonations. Exp. Mech. **40**(2), 219–225 (2000)
4. Singh, M., Suneja, H., Bola, M.: Dynamic tensile deformation and fracture of metal cylinders at high strain rates. Int. J. Impact Eng. **27**(9), 939–954 (2002)
5. Elek, P., Jaramaz, S.: Modeling of fragmentation of rapidly expanding cylinders. Theor. Appl. Mech. **32**(2), 113–130 (2005)
6. Gold, V.M., Baker, E.L.: A model for fracture of explosively driven metal shells. Eng. Fract. Mech. **75**(2), 275–289 (2008)
7. Feng, J., Jing, F., Zhang, G.: Dynamic ductile fragmentation and the damage function model. J. Appl. Phys. **81**(1), 2575–2578 (1997)
8. Curran, D.R.: Simple fragment size and shape distribution formulae for explosively fragmenting munitions. Int. J. Impact Eng. **20**(1), 197–208 (1997)
9. Zhou, F., Molinari, J.F., Ramesh, K.: Analysis of the brittle fragmentation of an expanding ring. Comput. Mater. Sci. **37**(1), 74–85 (2006)
10. Arnold, W., Rottenkolber, E.: Fragment mass distribution of metal cased explosive charges. Int. J. Impact Eng. **35**(12), 1393–1398 (2008)
11. Grady, D.: Fragment size distributions from the dynamic fragmentation of brittle solids. Int. J. Impact Eng. **35**(12), 1557–1562 (2008)
12. Liang, M.Z., Li, X.Y., Qin, J.G.: Improved expanding ring technique for determining dynamic material properties. Rev. Sci. Instrum. **84**(6), 065114–065116 (2013)
13. Jones, D., Chapman, D., Eakins, D.: A gas gun based technique for studying the role of temperature in dynamic fracture and fragmentation. J. Appl. Phys. **114**(17), 173508–173512 (2013)
14. Zhang, L., Jin, X., He, H.: Prediction of fragment number and size distribution in dynamic fracture. J. Phys. D Appl. Phys. **32**(5), 612 (1999)
15. Mock Jr., W., Holt, W.H.: Fragmentation behavior of Armco iron and HF-1 steel explosive-filled cylinders. J. Appl. Phys. **54**(5), 2344–2351 (1983)
16. Pandolfi, A., Krysl, P., Ortiz, M.: Finite element simulation of ring expansion and fragmentation: the capturing of length and time scales through cohesive models of fracture. Int. J. Fract. **95**(1), 279–297 (1999)
17. Mott, N.F.: Fragmentation of shell cases. NATO ASI Ser. Ser. C **189**(1), 300–308 (1947)
18. Grady, D., Wilson, L., Reedal, D.: Comparing alternate approaches in the scaling of naturally fragmenting munitions. In: 19th International Symposium on Ballistics, Interlaken, Switzerland, pp. 591–597 (2001)
19. Hudaverdi, T., Kuzu, C., Fisne, A.: Investigation of the blast fragmentation using the mean fragment size and fragmentation index. Int. J. Rock Mech. Min. Sci. **56**, 136–145 (2012)
20. Grady, D., Olsen, M.: A statistics and energy based theory of dynamic fragmentation. Int. J. Impact Eng. **29**(1), 293–306 (2003)
21. Grady, D.: Fragmentation of expanding cylinders and the statistical theory of NF Mott. In: AIP Conference Proceedings, vol. 2, pp. 799–802. IOP Institute of Physice Publishing LTD (2002)
22. De Chant, L.J.: Validation of a computational implementation of the Grady-Kipp dynamic fragmentation theory for thin metal plate impacts using an analytical strain-rate model and hydrodynamic analogues. Mech. Mater. **37**(1), 83–94 (2005)
23. Grady, D., Benson, D.: Fragmentation of metal rings by electromagnetic loading. Exp. Mech. **23**(4), 393–400 (1983)
24. Glenn, L., Chudnovsky, A.: Strain-energy effects on dynamic fragmentation. J. Appl. Phys. **59**(4), 1379–1380 (1986)
25. Zhou, F., Molinari, J.F., Ramesh, K.: A cohesive model based fragmentation analysis: effects of strain rate and initial defects distribution. Int. J. Solids Struct. **42**(18), 5181–5207 (2005)
26. Rusinek, A., Zaera, R.: Finite element simulation of steel ring fragmentation under radial expansion. Int. J. Impact Eng. **34**(4), 799–822 (2007)

27. Satapathy, S., Landen, D.: Expanding ring experiments to measure high-temperature adiabatic properties. Int. J. Impact Eng. **33**(1), 735–744 (2006)
28. Cohen Jr., E.A.: New formulas for predicting the size distribution of warhead fragments. Math. Modell. **2**(1), 19–32 (1981)
29. Hopson, M., Scott, C., Patel, R.: Computational comparisons of homogeneous and statistical descriptions of AerMet100 steel subjected to high strain rate loading. Int. J. Impact Eng. **38**(6), 451–455 (2011)
30. Kong, X., Wu, W., Li, J.: A numerical investigation on explosive fragmentation of metal casing using smoothed particle hydrodynamic method. Mater. Des. **51**(1), 729–741 (2013)
31. Levy, S., Molinari, J.F., Vicari, I.: Dynamic fragmentation of a ring: predictable fragment mass distributions. Phys. Rev. E Stat. Nonlinear Soft Matter Phys. **82**(6), 066105 (2010)
32. Grady, D., Kipp, M.: Geometric statistics and dynamic fragmentation. J. Appl. Phys. **58**(3), 1210–1222 (1985)
33. Grady, D.: Fragmentation of Rings and Shells: The Legacy of NF Mott. Springer, Berlin (2007)
34. Held, M.: Fragment mass distribution of he projectile. Propellants Explos. Pyrotech. **15**, 254–260 (1990)
35. Sil'vestrov, V.: Application of the Gilvarry distribution to the statistical description of fragmentation of solids under dynamic loading. Combust. Explos. Shock Waves **40**(2), 225–237 (2004)
36. Zecevic, B., Terzic, J., Catovic, A.: Characterization of distribution parameters of fragment mass and number for conventional projectiles. In: 14th Seminar on New Trends in Research of Energetic Materials, Pardubice, Czech Republic, pp. 1206–1039 (2011)
37. Hiroe, T., Fujiwara, K., Hata, H.: Deformation and fragmentation behaviour of exploded metal cylinders and the effects of wall materials, configuration, explosive energy and initiated locations. Int. J. Impact Eng. **35**(12), 1578–1586 (2008)
38. Pike, A., Zuo, Q.: Geometric design consideration for controlled fragmentation of metallic shells. Finite Elem. Anal. Des. **91**, 59–67 (2014)
39. Yang, Y., Li, X., Chen, S.: Effects of pre-notches on the self-organization behaviors of shear bands in aluminum alloy. Mater. Sci. Eng. A **527**(20), 5084–5091 (2010)
40. Liang, M., Li, X., Lu, F.: Effects of U-notches on the dynamic fracture and fragmentation of explosively driven cylinders. Theor. Appl. Fract. Mech. **77**, 50–58 (2015)
41. Goto, D., Becker, R., Orzechowski, T.: Investigation of the fracture and fragmentation of explosively driven rings and cylinders. Int. J. Impact Eng. **35**(12), 1547–1556 (2008)
42. Liang, M., Li, X., Lu, F.: Improved method used to investigate the dynamic shear failure of AISI 1045 steel cylinder under blast loading. Int. J. Appl. Mech. **08**(01), 1650003 (2016)
43. Li, X., Liang, M., Wang, M.: Experimental and numerical investigations on the dynamic fracture of a cylindrical shell with grooves subjected to internal explosive loading. Propellants Explos. Pyrotech. **35**(1), 1–10 (2014)
44. Chhabildas, L.C., Thornhill, T., Reinhart, W.: Fracture resistant properties of AerMet steels. Int. J. Impact Eng. **26**(1), 77–91 (2001)
45. Kipp, M., Grady, D.: Dynamic fracture growth and interaction in one dimension. J. Mech. Phys. Solids **33**(4), 399–415 (1985)
46. Lienau, C.C.: Random fracture of a brittle solid. J. Frankl. Inst. **221**(4), 485–494 (1936)